Supporting Online Material for

Organics Captured from Comet 81P/Wild 2 by the Stardust Spacecraft

Scott A. Sandford, Jérôme Aléon, Conel M. O'D. Alexander, Tohru Araki, Saša Bajt, Giuseppe A. Baratta, Janet Borg, John P. Bradley, Donald E. Brownlee, John R. Brucato, Mark J. Burchell, Henner Busemann, Anna Butterworth, Simon J. Clemett, George Cody, Luigi Colangeli, George Cooper, Louis D'Hendecourt, Zahia Djouadi, Jason P. Dworkin, Gianluca Ferrini, Holger Fleckenstein, George J. Flynn, Ian A. Franchi, Marc Fries, Mary K. Gilles, Daniel P. Glavin, Matthieu Gounelle, Faustine Grossemy, Chris Jacobsen, Lindsay P. Keller, A. L. David Kilcoyne, Jan Leitner, Graciela Matrajt, Anders Meibom, Vito Mennella, Smail Mostefaoui, Larry R. Nittler, Maria E. Palumbo, Dimitri A. Papanastassiou, François Robert, Alessandra Rotundi, Christopher J. Snead, Maegan K. Spencer, Frank J. Stadermann, Andrew Steele, Thomas Stephan, Peter Tsou, Tolek Tyliszczak, Andrew J. Westphal, Sue Wirick, Brigitte Wopenka, Hikaru Yabuta, Richard N. Zare, Michael E. Zolensky

*To whom correspondence should be addressed. E-mail: ssandford@mail.arc.nasa.gov

Published 15 December 2006, *Science* **314**, 1720 (2006)
DOI: 10.1126/science.1135841

This PDF file includes:

MATERIALS, METHODS AND SUPPORTING DATA

Introduction

For additional references that discuss the types of organic materials expected to be present in comets, see *(S1,S2)*. For additional references discussing the role comets may have played in the origin of life, see *(S3,S4,S5)*.

Particle Extraction Techniques

Whole tracks in the aerogel collectors were extracted using techniques developed in the Westphal lab at the Space Sciences Laboratory, U. C. Berkeley *(S6)*. Glass rods (1mm diameter) are pulled to make two microneedles. The needles are held by micromanipulators that are attached to the stage of the extraction microscope. The needles cut the aerogel by repetitive "poking." The micromanipulators are driven automatically by computer. First, an angled cut is made which undercuts the deepest feature of a particular impact; then a vertical cut is made around the impact. The resulting wedge-shaped block of aerogel (a "keystone") contains the entire impact track and the terminal particles. The keystone is then removed from the collector using silicon microforks that are inserted into pre-machined holes in the keystone. For certain analytical techniques, it is desirable to slice a track into multiple cross-sections; other techniques require a sample of the bulb that has been cleaved lengthwise. These specialized samples are prepared by laying a keystone on its side and using the same aerogel cutting tools to dissect or slice wafers of the track bulb. Terminal particles were removed from some keystones by using a bent glass needle to dig a tunnel to the particle and lifting it out using the same needle. The particle then can be mounted on a number of different types of substrates suitable for a variety of analytical techniques.

Since we had no a priori means of establishing which impact tracks might contain organic materials, most samples were simply allocated more-or-less randomly to Preliminary Examination Team (PET) members as they became available. In cases where early application of an individual analytical technique demonstrated a sample contained organics, it was then

possible to (i) subsequently allocate associated samples (for example, other particles from the same track) to other PET members, and/or (ii) pass the sample to another team member once the initial analysis was completed. By this process that we were able to examine a number of samples using multiple techniques.

Analytical techniques

Analytical techniques used to study the cometary samples and related control samples included:

Two varieties of two-step laser desorption laser ionization mass spectrometry *(S7,S8,S9),* called micro--L^2MS and ultra-L^2MS,

LC-FD/TOF-MS (Liquid Chromatography with UV Fluorescence Detection and Time of Flight Mass Spectrometry; *(S10)*),

STXM (Scanning Transmission X-ray Microscopy and C, N, and O XANES (X-ray Absorption Near Edge Structure) *(S11,S12,S13),*

Infrared and Raman Spectroscopy *(S14,S15,S16,S17,S18),*

IC (Ion chromatography with conductivity detection; *(S19)*),

TOF-SIMS (Time-of-Flight Secondary Ion Mass Spectrometry; *(S20)*), and

SIMS (Secondary Ion Mass Spectrometry; *(S21,S22)*).

Contamination Control and Assessment

The Sample Return Capsule (SRC) touched down on January 15, 2006 in the Utah Test and Training Range on soft mud in wet conditions under a prevailing crosswind. It bounced four times on different parts of the capsule before rolling a short distance and coming to rest on the side of its backshell. Visible inspection of the SRC shortly after impact indicated it had not suffered any identifiable loss of integrity. Nevertheless, since the SRC was not hermetically sealed, atmospheric gases in the environment surrounding the descending capsule would have been drawn into the capsule interior as it underwent pressure equalization. This provides a potential entry route for contamination by heatshield ablation products as well as water and soil from the landing site. To limit such contamination a high efficiency particulate air (HEPA) filter was fitted in-line between the backshell entry vents and the canister interior.

Atmospheric samples were collected from near the heatshield and backshell air entry vents shortly after the Recovery Team arrived, and several times thereafter as the SRC was transported to the clean room in which it was disassembled. GCMS analyses of the collected gases showed no significant contributions from organic compounds with the exception of 2-propanol and 1,1,1,2-tetrafluoroethane found in gases collected after the SRC was moved into a temporary cleanroom at the UTTR. These are thought to be associated with materials used earlier to prepare the clean room. Thus, there are currently no indications that significant amounts of volatile organic contaminants were sucked into the SRC through the back vents during descent. The Wild 2 samples were further protected from gas contaminants by a filter placed on the sample canister inside the SRC. During disassembly of the SRC, this filter was observed to look pristine, indicating that the SRC did not ingest any large amounts of 'smoky gas' or particulates. The lack of contamination by ablation gases will be more comprehensively verified when the canister filter is disassembled and its contents studied.

Soil samples were also obtained and analyzed from the various SRC impact locations, as well as along the 'roll track'. Using LC-FD/TOF-MS, a suite of amino acids were detected in the soil samples including aspartic and glutamic acids, serine, glycine, β-alanine, alanine, γ-amino-*n*-butyric acid (GABA), ε-amino-*n*-caproic acid (EACA), and valine. Methylamine (MA) and ethylamine (EA) were not detected in the soil samples above the part per billion level. XANES analyses of the soil from the Stardust landing sight demonstrated that the soil contained carbonate, potassium, and unsaturated, aliphatic carbon molecules. Chloride (by IC) was very abundant, as expected, reaching 32 ppt. Sulfate (also by IC) was observed at approximately 3 ppm). The organic material was associated with the potassium containing particles all of which were less than one micron in size. Very little mud stuck to the SRC.

It does not appear that the Wild 2 samples suffered any contamination from soil or water at the recovery site and currently no indications exist that ablative gases from the heatshield were ingested into the sample canister.

However, the possibility remains that some of the returned cometary samples could have been contaminated by organics emplaced during manufacture, testing, launch, and cruise of the spacecraft, as well as during sample curation. Additional contaminants could also be present in the aerogel medium used to capture the cometary samples, although NMR measurements indicate the primary form of contaminant carbon in the aerogel is in the form of Si-CH_3 groups. These issues were investigated and assessed by exposing, collecting, and analyzing a series of 'witness' coupons during key phases of the mission, and by characterizing unflown portions of the aerogel batches located in the Stardust collection trays. Particularly important in this regard is the Flight Aerogel Witness Tile, a tile of aerogel that was mounted on the collector tray deployment arm. This aerogel was placed so that it was protected from impacts during the comet flyby by the spacecraft's dust shields. Thus, this tile witnessed all the same environments (terrestrial and space) as the cometary collector tiles, but did not see the comet. It therefore represents an ideal control sample for our organics investigations. Results from the examination of this tile are discussed in the individual technique sections.

Tests of the Alteration of Organics when Fired into Aerogel

Tests using standards fired into Stardust-like aerogels at velocities near 6 km/sec suggest that the degree of alteration of organic materials is very dependent on the nature of the organic material and the matrix material in which the organics are bound. L^2MS studies of test shots of pure PAHs, like pyrene, show the impact distributes material all along the track, and even a few track widths into the surrounding aerogel, but show little evidence of oxidation or other alteration of the original PAH. Thus, materials of this sort may be partially volatilized, but do not appear to be altered.

In comparison, L^2MS studies of shots of Allende meteorite (CV3) material showed very little of the organic matter was volatilized and deposited along the impact track. Analysis of multiple terminal particles in the tracks showed that, while the overall abundance of PAHs was reduced somewhat, the actually mass distribution was remarkably similar to that characteristic of unshot bulk Allende (CV3) *(S23)*. Again, it appears that aromatic materials are not greatly altered by

impact into aerogel at these velocities, but that some material may be lost from the terminal particles.

In contrast, cocoa powder mixed with small soda-lime glass spheres and fired into aerogel shows a different behavior. In this case, essentially none of the original organics were found in association with the terminal soda-lime glass spheres; all the organic matter was found distributed along the bulb-shaped track and at least several track widths into the surrounding matrix (much like the shots of pure PAHs). However, in this case there was evidence of extensive alteration of some of the molecular components of the original cocoa powder, both in the form of bond-breaking and bond-creation. [NOTE: the segregation of organics and the glass in this case may explain why TEM analyses of removed grains show a relative dearth of organic materials adhering to mineral grains compared to what is seen for stratospheric IDPs].

Similar variations in the degree of alteration of organic materials fired into aerogels at these velocities are seen using other analytical techniques *(S24).*

Thus, one would anticipate that the organics in the collected cometary material could have undergone differing degrees of alteration ranging from little to no alteration all the way to extensive alteration, depending on the physical nature of the impacting particle and the chemical nature of the organics. Given the nature of many of the impacting particles (aggregates of smaller grains), it is possible that this entire range of degrees of alteration might be found in a single impact. In this respect, material in the tracks may share a characteristic of stratospheric IDPs, were individual particles can show evidence of severe heating and yet still retain some unmodified, less refractory materials. It should be noted, however, that the relatively heterogeneous and unequilibrated nature of many of the organics seen in the samples suggests that much of the material that has been examined has not been extensively altered by the collection process (see the main body of the paper).

Two-step laser desorption laser ionization mass spectrometry (L^2MS)

The L^2MS technique is ideally suited to the *in situ* detection of organic species that contain aromatic or π-conjugated systems *(S8)*. Such species, particularly in the form of the polycyclic aromatic hydrocarbons (PAHs), are believed to be ubiquitous in the interstellar and interplanetary environments *(S7,S15,S25)*. The L^2MS technique has been used to establish the presence of aromatic hydrocarbons in a wide variety of extraterrestrial materials including: meteoritic acid residues *(S26)*; carbonaceous and ordinary chondrites *(S27,S28)*; Martian meteorites *(S29)*; Antarctic micrometeorites *(S9)*; interplanetary dust particles *(S7)*; interstellar graphite grains *(S30)*; and interstellar ice analogs *(S31)*.

A detailed description of the μL^2MS technique has been presented in the literature *(S8,S26)* and is summarized here. Constituent neutral molecules of the sample are first desorbed with a pulsed infrared laser beam focused down to a spot, presently adjustable between 10 and 40 μm. Laser power density is maintained well below the plasma threshold to ensure desorption of neutral organic species with little or no fragmentation. A selected class of molecules in the desorbed plume is preferentially ionized by a single-frequency pulsed ultraviolet (UV) laser beam that passes through the plume. Resultant ions are then extracted and injected into a reflectron time-of-flight mass spectrometer and analyzed according to mass. A complete mass spectrum is obtained for each shot. The μL^2MS system at Stanford typically uses an ionization wavelength of 266 nm, which is strongly absorbed by the phenyl moiety and provides a selective ionization window for PAHs. The μL^2MS technique requires minimal sample processing and handling, and therefore allows analysis of samples with little possibility of contamination. Cometary impact tracks were exposed for μL^2MS surface analysis using the keystone extraction technique. All sample extractions were performed by Andrew Westphal, Christopher Snead, and Anna Butterworth in their UC-Berkeley Space Sciences Laboratory. In this technique, the track is dissected along its central axis *(S6)*. The resulting keystone was then mounted onto a brass sample platter using tape adhesive. Spatial analysis was performed using the Stanford University μL^2MS by rastering the laser desorption beam over the surface of the dissected track and using the NASA-JSC ultra-L^2MS to examine individual exposed particles. This results in complete mass spectra at each desorption spot (Fig S1 and S2).

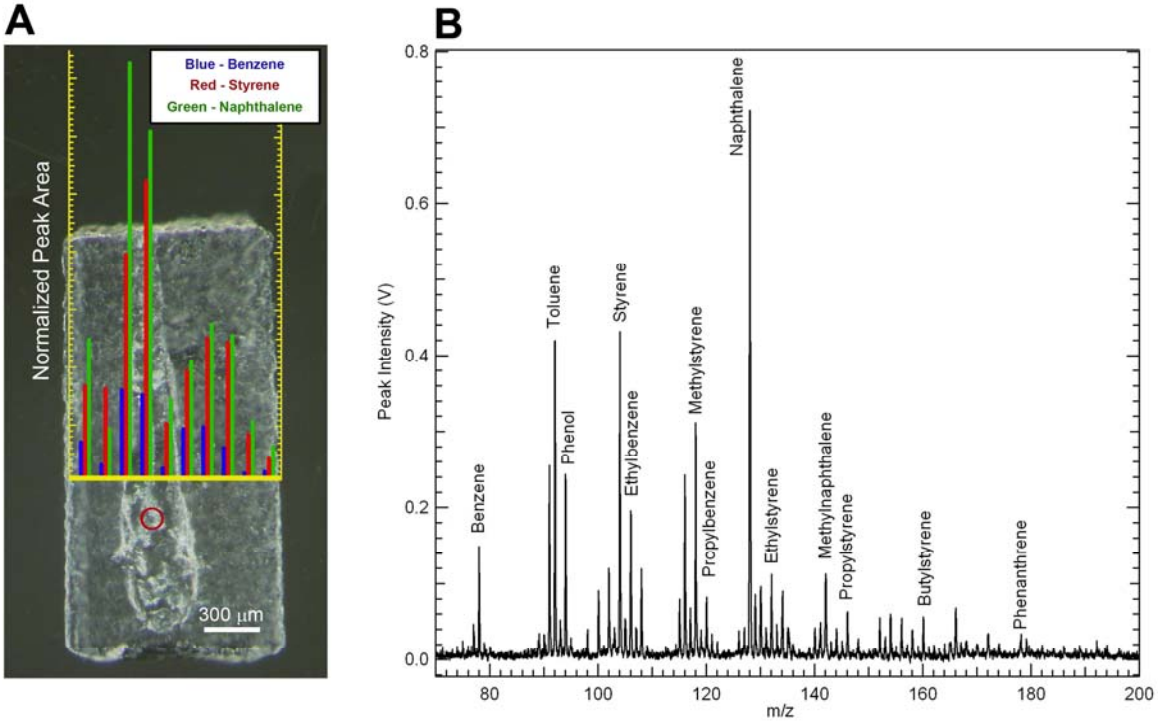

FIGURE S1 – µL^{2}MS of a cometary particle track in aerogel (Track 22): **(A)** the spatial distribution of three aromatic hydrocarbons whose intensities are plotted in a cross-section (in yellow) perpendicular to the cometary particle track. Aromatic molecules are found concentrated in the track, but also occur some distance on either side. **(B)** a mass spectrum taken within the cometary particle impact track at the location indicated by the red circle. Tentative peak identifications are listed near major mass peaks. This low-mass distribution of aromatic compounds is typical of the entire track.

Low-mass PAH distributions are seen in flight aerogel not associated with impact tracks. The flight Aerogel Witness Coupon, an aerogel tile that was exposed to everything the rest of the tray was exposed to *except* the comet, showed even weaker PAH backgrounds. Both non-track cometary aerogel and the witness coupon aerogel show only a very weak indication of PAHs except at very high laser desorption powers. At high powers the µL^{2}MS CO_2 laser was observed to make a visible hole in aerogel samples and a stronger aromatic signature resulted. The presence of strong aromatic signals consistently correlated with the creation of a hole. No correlation between aromatic abundance and depth into the witness coupon was observed, indicating that the source of this material is distributed throughout the tile. At these higher powers both the cometary aerogels and the witness coupon produced identical aromatic

signatures, indicating that this material is *neither cometary nor contamination introduced during space flight*. At these high powers, it is likely that the majority of the PAHs being seen in aerogel are due to pyrolysis of carbon in the original aerogel tiles. It is possible that these PAHs could also be created during the high energy impact of a small particle.

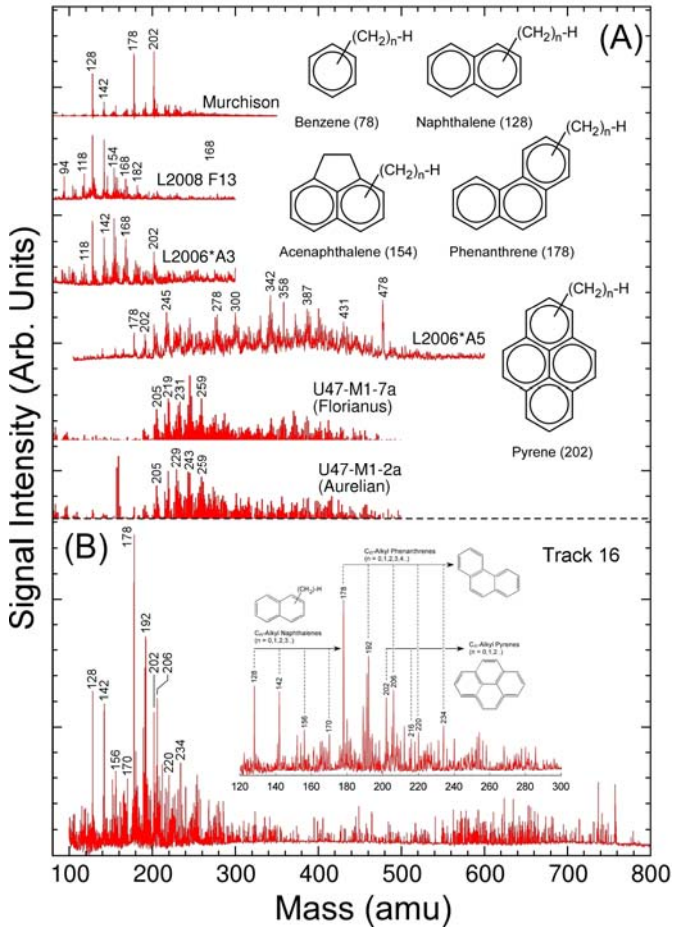

FIGURE S2 – (A) The L^{2}MS spectra of the carbonaceous chondrite Murchison and 5 stratospheric IDPs *(7)*. The meteorite and some IDPs show relatively simple populations dominated by small PAHs, but the spectra of some IDPs extend to higher masses, indicating a more complex distribution of PAHs. (B) The L^{2}MS spectrum of Stardust sample Track 16, is similar to the lower IDP spectra in 1A. The higher mass envelope of peaks above 300 amu for the Stardust sample probably reflects increased polymerization during impact with the aerogel compared to the more benign atmospheric deceleration experienced by most stratospheric IDPs.

Time-of-Flight Secondary Ion Mass Spectrometry (TOF-SIMS)

A TOF-SIMS IV instrument from ION-TOF was used in this study. The instrument is equipped with a pulsed gallium liquid metal ion source producing primary ions with 25 keV energy. Sample charging due to the primary ion beam is effectively compensated by bombardment with low-energy electrons between consecutive primary ion pulses. This allows all different types of Stardust samples to be studied without special sample preparation: crater residues on aluminum foil, dissected aerogel keystones displaying particle tracks, and extracted particles that were embedded in epoxy and sliced with a microtome. Since elements, isotopes, and organics as well as their lateral distribution were measured simultaneously in a single analysis, all measurements of Stardust samples were performed at high lateral (~0.2 µm) and high mass resolution ($m/\Delta m_{FWHM}$ > 4000 at mass 29 amu for rough surfaces like Al foil craters or aerogel tracks and ~5500 for flat surfaces like microtomed particles). Further details on TOF-SIMS technique are given in the literature *(S20)*.

TOF-SIMS detected PAHs that were clearly correlated to cometary material or impact feature as exemplified by a PAH secondary ion distribution image of a cometary impart crater found in aluminum foil sample C2009N (Fig S3b,c).

TOF-SIMS measurements of PAHs typically show fragmentation of PAHs. In most cases the $C_9H_7^+$ secondary ion has the highest abundances among all PAH ion peaks. The abundances of different sized PAHs relative to the abundance of $C_9H_7^+$ are similar for PAHs in tracks and terminal particles in aerogel, but show a flatter distribution in the residues found in craters in aluminum foil (Fig S3a). This may be a fractionation effect associated with a greater loss of small PAHs in the foil impacts.

PAHs from particles of the carbonaceous chondrite Allende shot into aerogel and analyzed in a dissected keystone *(S32)* show a size-abundance distribution of PAHs that is very similar to that seen in the cometary samples collected in aerogel. PAHs from the carbonaceous chondrites Murchison and Orgueil meteorites show a somewhat higher relative abundance of heavier PAHs (see Fig S3a; *(S33)*).

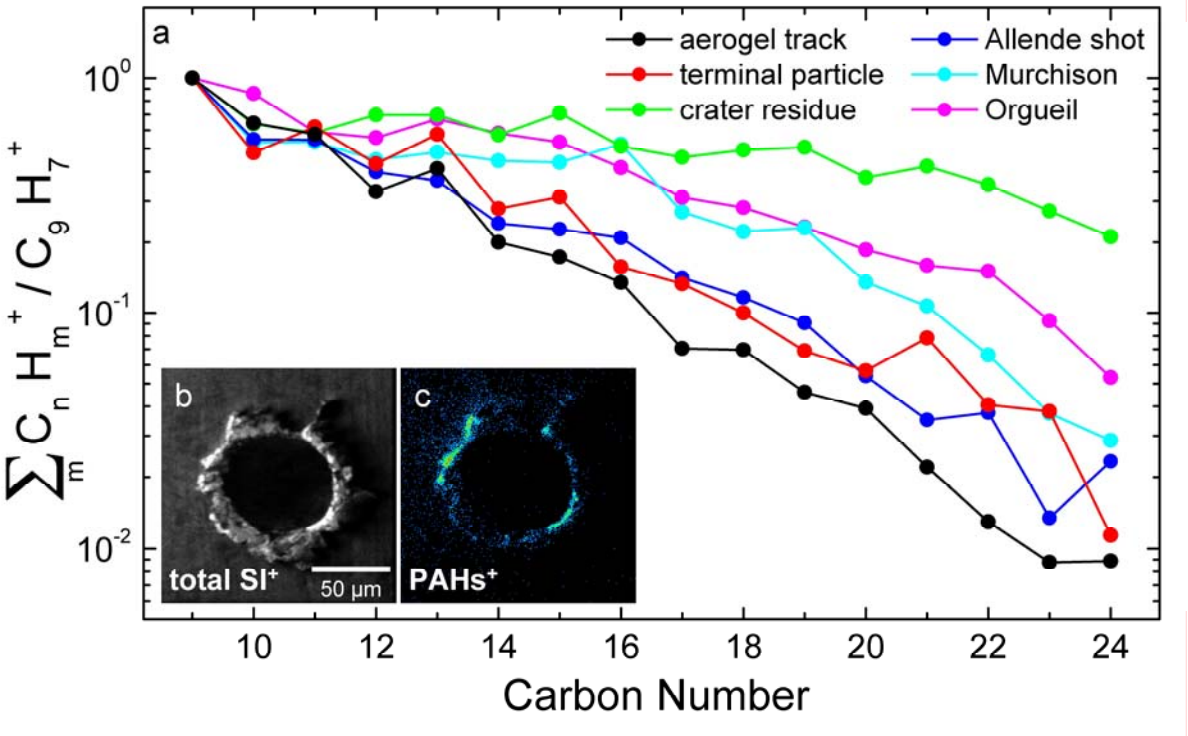

FIGURE S3 – (a) Abundances of PAHs in Stardust samples as a function of their number of carbon atoms relative to the abundance of $C_9H_7^+$, the PAH fragment that typically shows the highest intensity in TOF-SIMS analysis. Analyzed samples include one dissected aerogel keystone with a particle track (Track 21), one terminal particle extracted from aerogel (Track 44, Grain 4), and residue from the rim of a crater in aluminum foil (large crater from C2009N). For the latter, the corresponding PAH secondary ion distribution image (c) and a total secondary ion image (b) are shown. For comparison, data are also shown for Allende material shot into aerogel *(33)* and two carbonaceous meteorites, Murchison and Orgueil *(34)*.

Raman Spectroscopy

Raman spectra taken at the Osservatorio Astrofisico di Catania in Italy were taken from grains extracted from aerogel and deposited as bulk particles on KBr windows mounted in a special sample holders designed to allow combined micro-IR, micro Raman, FESEM, and EDS analyses without the need for sample manipulation in the laboratory *(S18)*. A Cu finder grid, with a central 300 µm hole was used to help localize the particle's location. A polycarbonate probe clip was placed over the Cu grid to serve as a clean shield to prevent spurious dust deposition and other contamination.

Raman spectra of 3 grains (Track 35, Grain 16; Track 35, Grain 18; and Track 35, Grain 20) were taken using a continuous multiline Ar ion laser beam at 514.5 nm wavelength. A confocal microscope (DILOR) focuses the laser beam onto the particle in a 1 μm diameter spot with a power mostly maintained at 0.03 mW and always lower then 0.1 mW. The Raman scattered light arising from the illuminated spot is collected by the same objective and is collimated into a parallel beam that is reflected back along the same path as the laser. The Raman scattered light is then focused on the entrance slit of the triplemate spectrometer (SPEX) equipped with a CCD detector. This confocal system makes it possible to perform measurements on samples with negligible performance losses.

Raman analyses at the Carnegie Institution of Washington were performed with a multi-function scanning probe microscope of the Geophysical Laboratory. The instrument, a WiTec (Germany) α-SNOM, includes near-field optical microscopy, atomic force microscopy and confocal Raman microscopy (532 nm frequency-doubled Nd:Yag laser). The instrument allows non-destructive Raman characterization of samples at sub-μm spatial resolution (typically ~400 nm with 100x short working distance optical microscope). Spectral images were acquired, where each pixel contains a full Raman spectrum (1024 channels, 600 gratings/mm, ~4 cm^{-1} spectral resolution). The Raman data cube was reduced using custom software. Tests have shown that meteoritic insoluble organic matter has not been significantly altered during the analyses, due to the laser-induced heating at low power (55 μW) and the fast measurements (typically 4 sec/pixel). Excessive fluorescence overwhelming Raman spectral features has been overcome with the use of confocal optics. All samples (Track 13, Grain 1; Track 35, Grain 25; Track 35, Grain 27; Track 17, Grain 1) were pressed into gold and most particles were subsequently analyzed with SIMS (Track 17, Grain 1 was analyzed after the SIMS measurements).

Laser Raman analyses were conducted at PSSRI, Open University, on Samples Track 35, Grain 1, and Track 35, Grain 28. These samples were particles (aerogel with some cometary material) extracted and pressed into gold foil at NASA-JSC. Laser Raman data were taken with a fully confocal Horiba Jobin Yvon Labram HR Raman system. The laser, a 514 nm argon ion laser, delivered a power at the sample surface of 180 μW (Track 35, Grain 28) and 60 μW (Track 35,

Grain 1). The beam was focused with a x100 long working distance objective giving a spatial resolution of approx 1.2 μm. Spectra were recorded across the whole of each particle with a 1.5 μm step in both x and y. Spectra were accumulated as 5 sets of 30-second integrations. The 800 mm spectrometer coupled with a low resolution grating gives a dispersion of 2 cm^{-1} per pixel on the CCD detector at 514 nm. The instrument was calibrated for absolute laser wavenumber and Raman shifts before analyses. The steep sloping fluorescence baseline was subtracted and the D and G features fitted with a Gaussian-Lorentzian model.

Raman spectra obtained by the Orsay–IAS group were taken from grains extracted from aerogel and pressed as bulk particles on gold windows, allowing, without the need for sample manipulation, combined micro-IR, micro Raman, FESEM, and EDS non destructive analyses and followed by a NanoSIMS investigation of the same grains. The Raman instrument is a Labram HR800 Horiba Jobin-Yvon (national facility equipment at ENS Lyon). Excitation is delivered by an argon ion laser (514.5 nm) and the spectral resolution is of 1 cm^{-1} when using a 1800 gr/mm grating. The laser power at the sample surface did not exceed 0.1 mW. The spatial resolution is 1 μm when using a x100 Olympus objective. The analytical procedure consists in fitting the D and G bands with two Lorentzian bands and a linear baseline.

Raman measurements at Washington University in St. Louis were performed on sample Track 35, Grain 30 that was pressed into Au at NASA-JSC (Fig S4). The instrument used is an integrated, fiber-optically coupled microscope-spectrometer-detector system (HoloLab Series 5000 Raman Microscope from Kaiser Optical Systems, Inc). This instrument has no moving parts and is based on an axial spectrometer with holographic gratings that allows for very good photon efficiency and wavelength accuracy. Raman excitation light of 532 nm is delivered by a frequency-doubled Nd-YAG laser that was coupled into a Leica microscope via a 8 μm single mode optical fiber. A 80x ULWD objective with NA of 0.75 and a working distance of 8 mm was used for focusing the light onto the sample, which resulted in a spatial resolution of ~1 μm. The laser power at the surface of the sample was less than 500 μW. The spectral range of 100-4000 Δcm^{-1} was simultaneously detected with a thermoelectrically-cooled CCD array detector with 2048 channels and a spectral resolution of 2.5 cm^{-1}. Spectral acquisition time was 64 x 4 seconds per spectrum. Data acquisition, intensity and wavelength calibration, as well as filtering

were controlled by the HoloGrams software. Peaks were deconvolved with a mixed Gaussian-Lorentzian algorithm without any baseline correction.

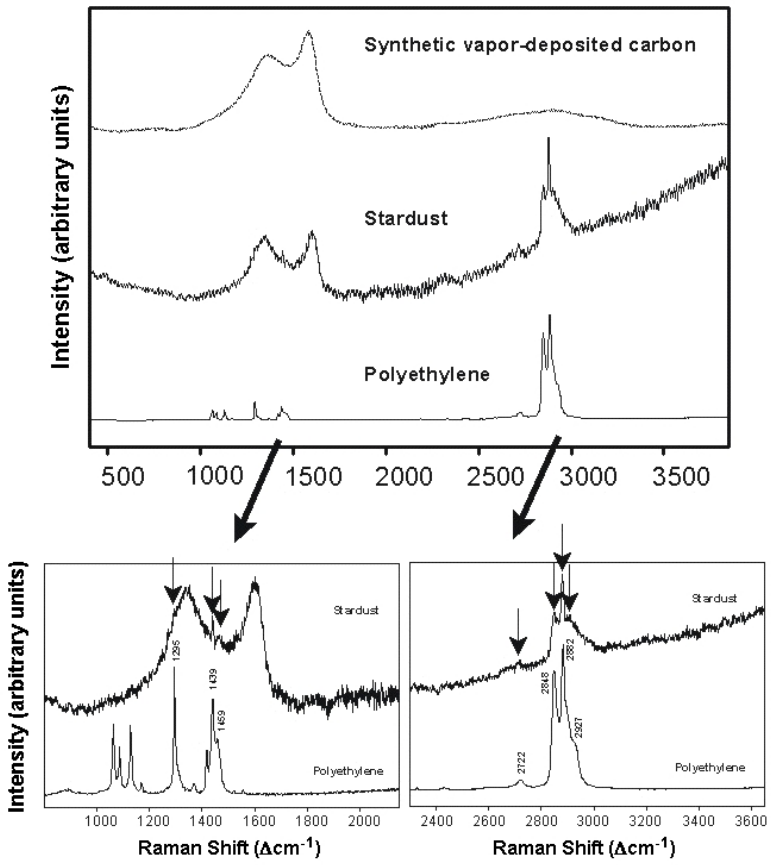

FIGURE S4 – The background corrected spectrum of the Stardust particle (Track 35, Grain 30) shows bands for both aromatic and aliphatic carbonaceous materials. The two very broad bands centered at ~1360 Δcm^{-1} (D band) and ~1590 Δcm^{-1} (G band) are caused by aromatic C-C vibrations characteristic of large PAHs or in kerogen-like materials. While the Raman data of Stardust samples are uniformly dominated by the aromatic G and D bands, this particle was seen to also produce strong C-H stretching vibration peaks at 2848 and 2882 Δcm^{-1}, and a weak band at 1439 Δcm^{-1}. These features are consistent with the presence of alkane-type saturated hydrocarbons, as exemplified by comparison with the spectrum of polyethylene. Similar aliphatic features were also seen in Raman spectra of two additional Stardust samples (Track 35, Grain 32 and Track 41, Grain 11 generally seen in Raman spectra of Stardust samples.

Infrared Spectroscopy

Infrared spectra were obtained from the infrared microspectroscopy beamline 1.4.3 at the Advanced Light Source, Lawrence Berkeley National Laboratory. This beamline was used to map distribution of organics in and around particle tracks within aerogel keystones. The beamline is equipped with a ThermoNicolet Magna 760 FTIR bench and a SpectraTech Nic-Plan IR microscope. The synchrotron source was focused to a diffraction-limited spot and aligned with the optical beam path. For the measurement of the -CH_2- and –CH_3 peaks this corresponds to a spot size of ~3 μm. A KBr beamsplitter was placed in the beam path and the transmitted light was collected with an MCT-A detector between 650 and 4000 cm^{-1} with 4 cm^{-1} spectral resolution. Spectra were normalized to the air spectrum and typically collected between 6-60 sec/point. Aerogel keystones (100-200 μm thick) were held with microtweezers and placed directly under the microscope. The sample, mounted on a special sample holder, was moved on a microscope stage with sub-micrometer precision while the beam remained fixed during data collection of the maps.

Infrared spectra were also acquired at the Osservatorio Astronomico di Capodimonte in Italy with a microscope attached to a FTIR interferometer (Mod. Bruker Equinox-55) in the range 7000-600 cm^{-1} with a spectral resolution of 4 cm^{-1}. Comet Wild 2 particles (Track 35, Grain 16; Track 35, Grain 18; Track 41, Grain 7, and Track 41, Grain 10) were placed on a special sample holder *(S18)* and spectra acquired in transmission. Due to diffraction limits, the smallest infrared beam focused on the samples was 20 μm spot. This was larger then the average size (about 10 μm) of the analyzed particles. Thus, spectra of overall bulk particles were obtained.

FTIR spectra obtained by the Orsay–IAS group were taken from the same grains from which Raman spectra were acquired. The instrument is a NicPlan microscope associated with the Magma 860 FT-IR spectrometer equipped with MCT detectors and used in the reflection mode. The IR source is an internal globar type source; KBr beamsplitters are available in the 5000–500 cm^{-1} range. The wavelength/wavenumber coverage is 2.5–15.4 μm (4000–650 cm^{-1}) with a spectral resolution of 4 cm^{-1}. The smallest IR beam focused on the samples was around 15 μm, the approximate size of the samples.

Fig S5 shows the 4000-1500 cm^{-1} infrared spectrum of sample Track 59. This spectrum contains features due to both sample material and aerogel. Calculating the relative abundance of functional groups detected in the IR spectra, particularly the $–CH_2-$ and $–CH_3$ groups, requires that absorption contributions from the aerogel be removed. This can be done by subtracting the spectrum of aerogel far from a track to the sample spectra. Fig S6 shows an example where this has been done in the OH and CH stretching region. The corrected spectrum shows an aliphatic CH stretching feature centered near 2900 cm^{-1} that is clearly dominated by $–CH_2-$ groups. A weak aromatic CH stretching band is also seen near 3055 cm^{-1}. Since aromatic structures can have relatively low H coverage (particularly compared to aliphatic materials), the relative weakness of this feature does not necessarily imply low abundances of this material.

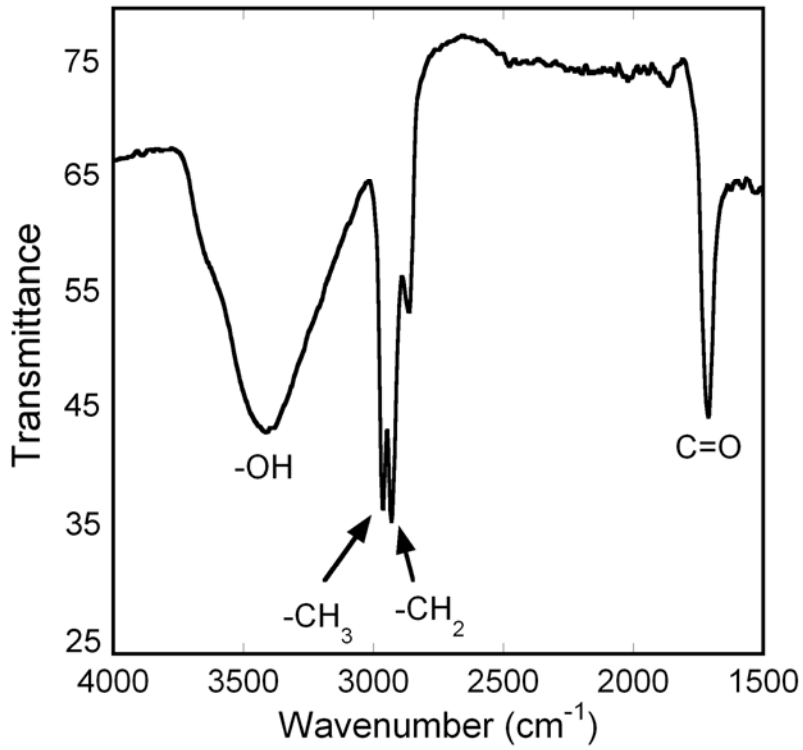

FIGURE S5 – The 4000-1500 cm^{-1} infrared spectrum of a section of Track 59. Absorption features can be seen near 3322 cm^{-1} (–OH), 2968 cm^{-1} ($-CH_3$), 2923 cm^{-1} ($–CH_2-$), 2855 cm^{-1} ($-CH_3$ and $–CH_2-$), and 1706 cm^{-1} (C=O). All these features except the 1706 cm^{-1} C=O band contain some contributions from aerogel.

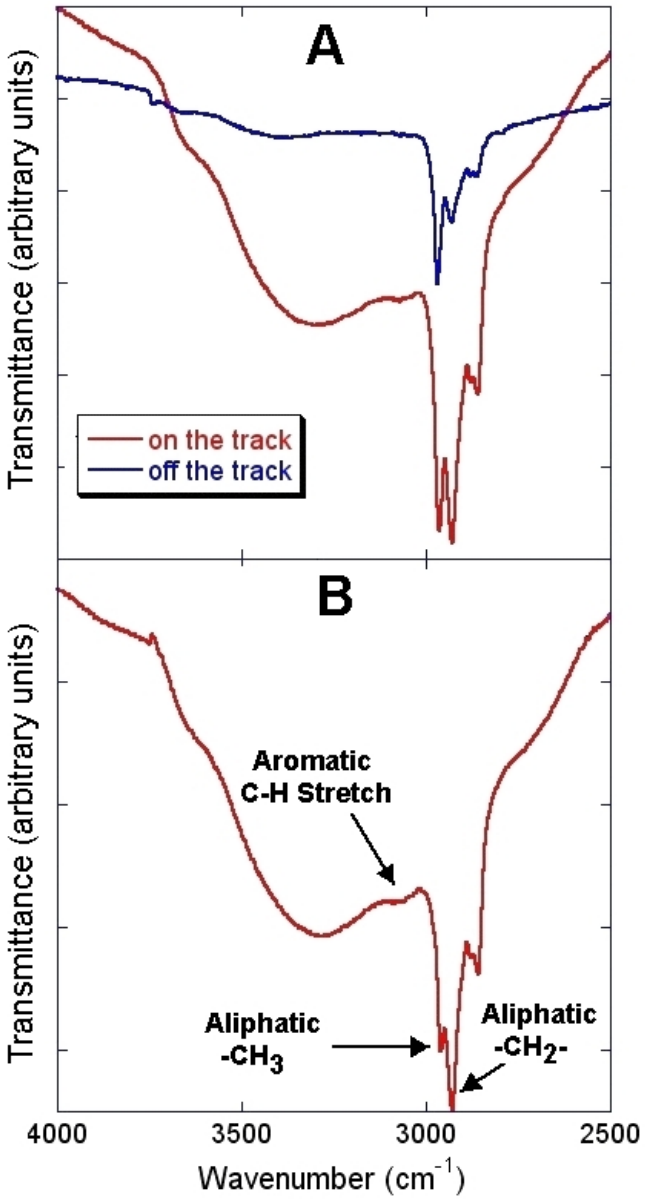

FIGURE S6 – (A) The 4000-2500 cm^{-1} spectrum from an aerogel keystone (Track 58) on a track (red line) and far from the track (blue line). The aerogel spectrum can be scaled using an absorption feature due solely to aerogel and subtracted from the track spectrum. The residual absorption (B) is then dominated by new, non-aerogel material associated with the track dominated by a broad feature near 3300 cm^{-1} (-OH) and narrower features near 3065 cm^{-1} (aromatic CH stretch, weak), 2968 cm^{-1} ($-CH_3$ asymmetric stretch), 2923 cm^{-1} ($-CH_2-$ asymmetric stretch), and 2855 cm^{-1} (symmetric $-CH_3$ and $-CH_2-$ stretches).

Scanning Transmission X-ray Microscopy and X-ray Absorption Near Edge Structure (STXM/XANES)

XANES of ultramicrotomed sections of particles extracted from aerogel were performed on three different STXMs located at beam lines 5.3.2 and 11 at the Advanced Light Source, Lawrence Berkeley Laboratory, and beam line X1A at the National Synchrotron Light Source, Brook Haven National Laboratory. XANES analyses can provide information regarding the oxidation state and bonding environments of low Z elements (C, N, and O). When combined with STXM, micro-XANES may be acquired at spatial resolutions down to 100's of nanometers *(S12)*, thus affording a unique opportunity to explore organic chemical variation in retrieved aerogel particles. Also, by using a method where a series of x-ray images taken at incremental differences in the photon energy are collected and spatially aligned, one can obtain spectra from regions as small as the spatial resolution of the microscope (30 nm) *(S34)*.

The Scanning transmission x-ray microscopes used in this study use coherent radiation from a synchrotron light source, ranging in energy from 100-1500 eV. This light is monochromatized and focused to a spot using a Fresnel zone plate. The typical focus spot for this work was 30 nm. The sample is scanned through the focus and the transmitted intensity is recorded by a large area detector, resulting in an absorption contrast image of the sample. The energy of the microscopes are well matched to the inner-shell electron binding energy of low Z elements, resulting in high absorption coefficients and high quality contrast images. Using spectromicroscopy, one can obtain a series of images of the same field taken at different energies around an element's absorption edge. From these energies at and away from an element's x-ray absorption near edge structure (XANES) resonances, different bonding states of that element can be identified. XANES spectroscopy corresponds to the transition of an electron from a core-level to an unoccupied virtual orbital or continuum and reflects the electronic state of the atom. Its capabilities are: 1. the detection of bonds (C-C, C=C, C=O, and C-H, to name a few); 2. the determination of bond lengths; and 3. crystal orientation *(S35)*.

The relative C, N, and O abundance of the XANES samples can be determined by measuring the X-ray absorption intensity above the respective C-, N-, and O- 1s ionization edges, which

correlates with the atomic density of each element in the sample. This works well if there is no significant contributions in the absorption spectra from other elements having binding energies from other electron shells besides the K shell. Fig S7 shows C-, N-, and O- 1s ionization edge spectra of a Stardust sample.

Materials with the high O/C and N/C ratios typical of the organic materials examined by XANES are likely to be relatively labile, and there is ample evidence seen for this. First, of course, is the observation from infrared spectroscopy that organics have been injected into the aerogel surrounding many of the impact tracks. In addition, in the case of XANES measurements, a number of instances were observed in which the organic material, or a portion of it, disappeared as it was measured in the X-ray beam. This was observed during measurements with higher X-ray fluences. Similar behaviors were also seen in other beam instruments (for example, Nano-SIMS). Also, in one case (a thin section from Track 35, Grain 16, Mount 4), evidence is found for organic matter that diffused out of the original particle and into the surrounding epoxy in which the particle was embedded for microtoming, suggesting that a portion of the organics are soluble in epoxy.

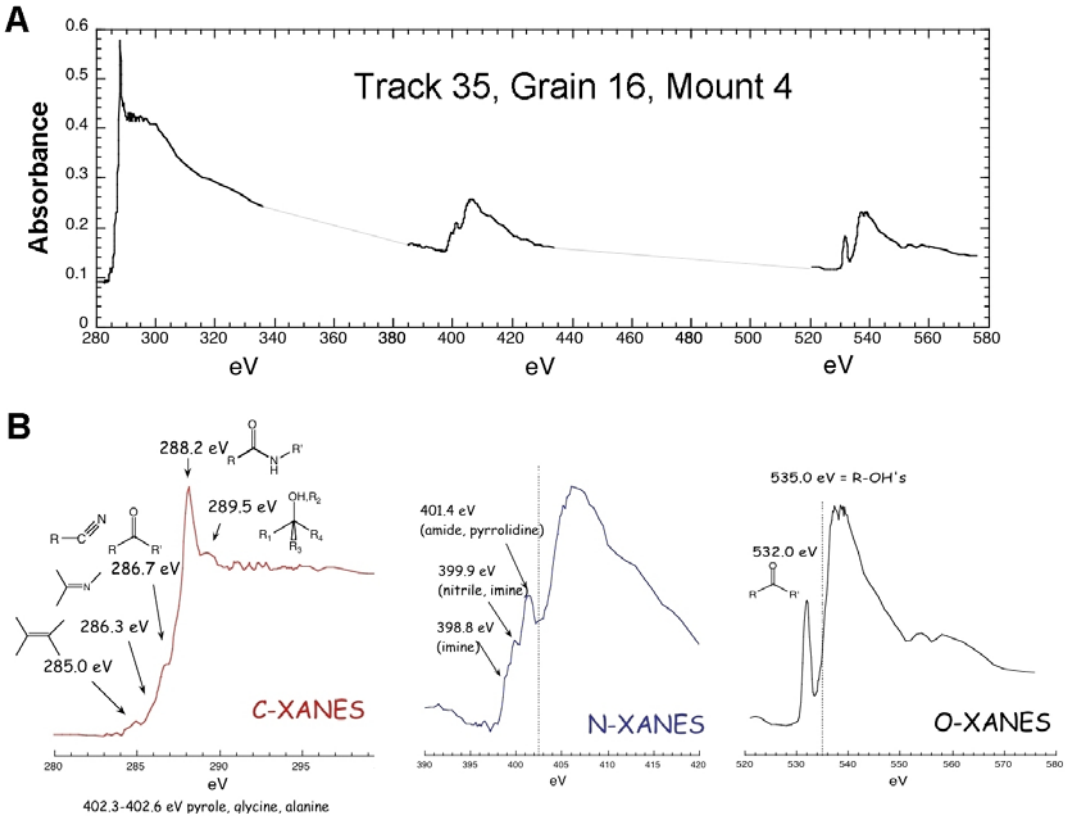

FIGURE S7 – (A) A XANES spectrum showing the C-, N-, and O- 1s ionization edges of Track 35, Grain 16, Mount 4 to scale. The relative intensity of each edge at energies beyond each near edge region is directly related to the relative atomic abundance of each element. (B) Expanded spectra of the individual C, N, and O edges revealing the near edge spectral features associated with different organic functional groups.

Liquid Chromatography with UV Fluorescence Detection and Time of Flight Mass Spectrometry (LC-FD/TOF-MS)

We investigated the abundances of amino acids and amines, as well as their enantiomeric composition, in Stardust flight aerogels (Cell 2054, Aerogel Fragment 4, hereafter C2054,4, and Cell 2086, Aerogel Fragment 1, hereafter C2086,1) using high performance liquid chromatography with simultaneous UV fluorescence and time of flight-mass spectrometry

detection (LC-FD/TOF-MS). The LC-FD/TOF-MS were identical to those described in *(S10)*. Three pieces (1-3) of the C2054,4 were cut from the original slab (Fig S8) and weighed separately with masses of 5.2 mg, 7.6 mg, and 8.7 mg, respectively. Piece 3 was located directly under and adjacent to Piece 5, which contained Track 25 (Fig S8). C2086,1 weighed 3.2 mg and was taken from Tile C2086 from a location that was not adjacent to any visible impact tracks. As controls, procedural blanks and several Stardust aerogel samples, including a 14 mg piece of preflight aerogel (Flight Spare Aerogel Cell E243-13C, unflown) that had been kept sealed under vacuum since original bakeout in 1998 and a 0.2 mg sample of the aerogel witness coupon (WCARMI1CPN,9), were carried through the same extraction protocol. The aerogel samples were heated inside a sealed glass ampoule containing 1 mL Millipore water (18 MΩ) at 100ºC for 24 h. The water extracts were dried under vacuum and half of each extract was then hydrolyzed under 6M HCl vapor at 150ºC for 3 h. Both acid hydrolyzed and non-hydrolyzed aerogel water extracts were derivatized with *o*-phthaldialdehyde/*N*-acetyl-L-cysteine (OPA/NAC) and analyzed for primary amines using LC-FD/TOF-MS.

The most abundant primary amine compound detected in the Stardust flight aerogels is ε-amino-*n*-caproic acid (EACA); its most likely origin is exposure to Nylon-6 *(S10)*. Several other amines including glycine, β-alanine (BALA), γ-amino-*n*-butyric acid (GABA), L-alanine, ethanolamine (MEA), methylamine (MA), and ethylamine (EA) were also identified in the aerogels (Fig S8). The absence of D-amino acids and the similarity in amine distribution between the comet exposed C2054,4 sample and the witness coupon indicates that most of the amines are terrestrial in origin (Fig S8). The enhanced relative abundances of MA, EA, and possibly glycine in both comet-exposed aerogel samples compared to the preflight and witness coupon aerogels suggest a cometary origin for these compounds (Fig S9). Compound specific isotopic analyses of these amines will be necessary to constrain their origin.

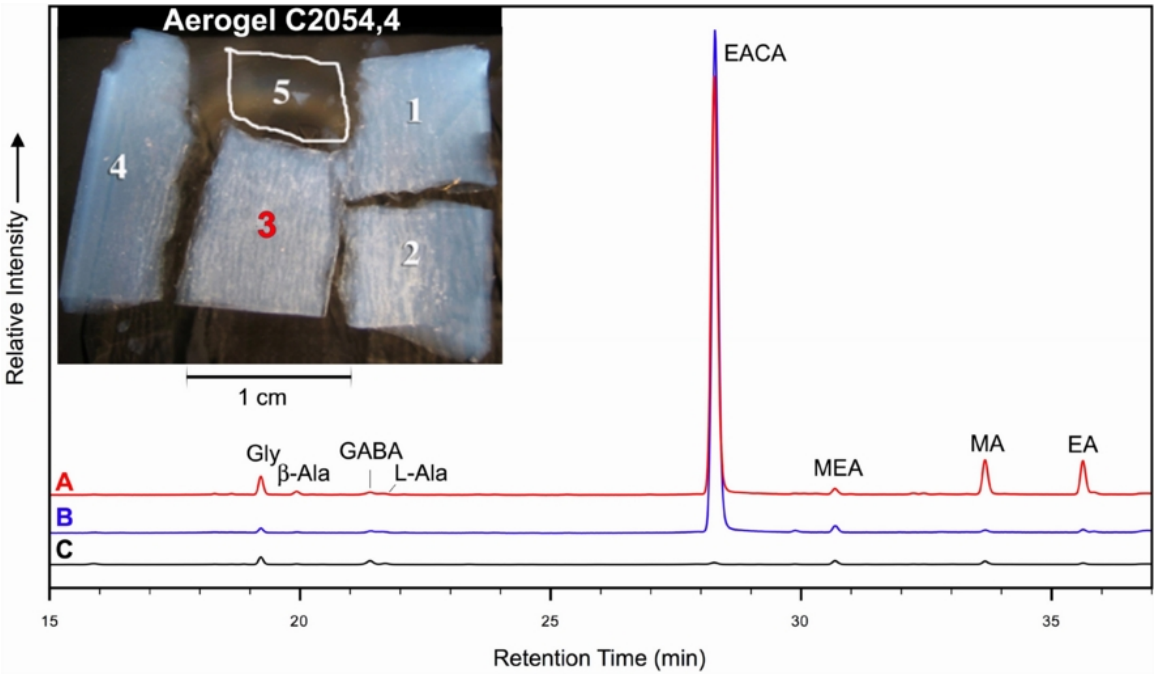

FIGURE S8 - The fluorescence chromatograms from LC-FD/TOF-MS analyses showing the amines detected in: (A) Stardust comet exposed aerogel C2054,4-Piece 3; (B) Stardust aerogel witness coupon WCARMI1CPN,9; and (C) preflight aerogel (Flight Spare Aerogel Cell E243-13C, unflown). Peak identities were established by comparing retention time with authentic standards and measuring the positive electrospray exact mass of each identified peak. The inset shows the C2054,4 cutting diagram oriented with the comet-exposed surface at the top. MA and EA were detected in aerogel Pieces 1-3 at levels that exceeded those found in the aerogel witness coupon and preflight aerogel. There was no significant difference in MA and EA abundances between Pieces 1 and 2 to suggest a concentration gradient with depth. Pieces 4 and 5 (which contained Track 25) were not analyzed by this technique.

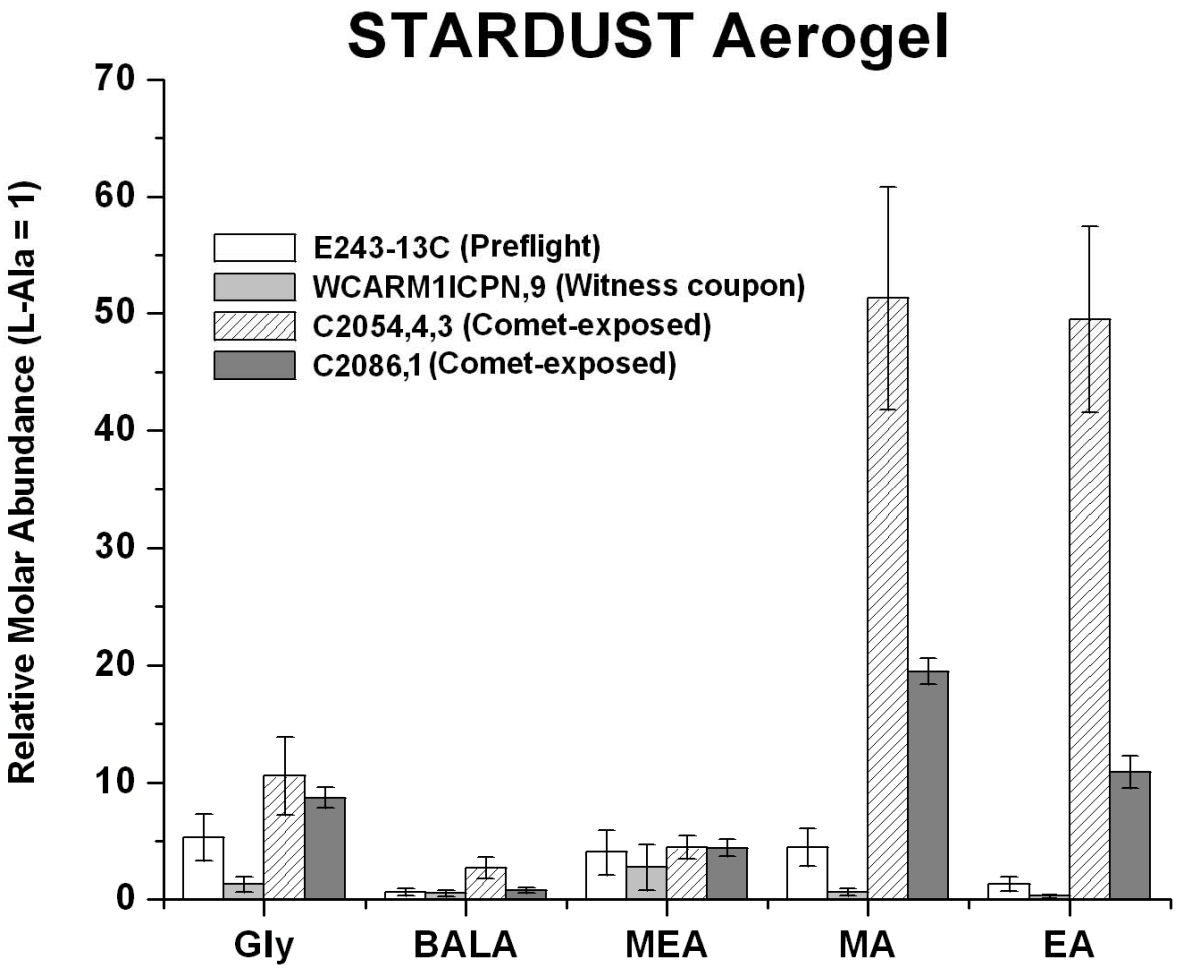

FIGURE S9 - A comparison of the relative molar abundances (L-Ala = 1) of glycine (Gly), β-alanine (BALA), ethanolamine (MEA), methylamine (MA), and ethylamine (EA) in the acid-hydrolyzed hot-water extracts of Stardust aerogel. The high relative abundances of MA, EA, and glycine in comet-exposed aerogel samples C2054,4 (Piece 3) and C2086,1 compared to the preflight (E243-13C) and witness coupon (WCARM1ICPN,9) aerogel samples suggest a cometary origin for these amines.

Secondary Ion Mass Spectrometry (SIMS)

Hydrogen isotopes were measured along with C using a Cameca ims-6f ion microprobe, in scanning imaging mode. A focused <10pA Cs^+ ion beam was rastered across samples with synchronized collection of secondary ions. Techniques were identical to those described in *(S36)*. All but one analyzed sample were extracted from the aerogel collectors and pressed into Au foils. A 500 nm thick slice of sample Track 13, Grain 1, prepared by ultramicrotome, was placed directly on a Au foil. Data were quantified using custom image processing software and terrestrial standards.

Chemical maps of Stardust samples were produced with the Cameca NanoSIMS 50 of the Muséum National d'Histoire Naturelle in Paris. Samples were placed on a gold foil. Using a focused primary beam of Cs^+, secondary ions of $^{12}C^-$, $^{12}C^{14}N^-$ and $^{32}S^-$ were sputtered from the sample surface and detected simultaneously (multicollection-mode) in electron-multipliers at a mass-resolving power of ~4500 ($M/\Delta M$). At this mass-resolving power, the measured secondary ions are resolved from potential interference. Because nitrogen is detected as CN^-, it can only be detected in the presence of carbon. Images were obtained from pre-sputtered surfaces by stepping the primary beam across the sample surface. The primary beam was focused to a spot-size of ~50-100 nm and the step-size was adjusted so that it was comparable to, but slightly smaller than the size of the primary beam. An electron gun supplied electrons to the sputtered surface during analysis in order to compensate positive charge deposition from the primary beam and minimize charging effects.

Calibrated N/C atomic ratios were obtained from the measured $^{12}C^{14}N^-$ and $^{12}C^-$ ratios by normalization to a kerogen standard from the Eocene Green River Shale. The kerogen was extracted by standard HF-HCl techniques and comprised $\geq$94% of the insoluble acid residue; it has an atomic N/C ratio of 0.025 (measured by standard chemical techniques), which was calibrated to the $^{12}C^{14}N^-/^{12}C^-$ ratios measured under NanoSIMS conditions identical to those used for analyzing the Stardust samples.

The Presence of Labile Organics

Several experimental groups observed the loss of organics in their samples over time when exposed to higher X-ray, laser, or ion beam fluences, providing further evidence of a relatively labile component of the organics. It is interesting to note that this may be one reason why organic grains appear to have low abundance in TEM sections *(S37)*.

References and Notes

S1. J. Kissel, F. R. Krueger, Nature 326, 755 (1987).

S2. M. J. Mumma, in Astronomical and Biochemical Origins and the Search for Life in the Universe, C. B. Cosmovici, S. Bowyer, D. Wertheimer, Eds. (Editrice Compositori, Milan, 1997), pp. 121-143.

S3. J. Oró, Nature 190, 389 (1961).

S4. E. Anders, Nature 342, 255 (1989).

S5. A. H. Delsemme, Advances in Space Research 12, 5 (1992).

S6. A. J. Westphal et al., Meteoritics Planetary Science 39, 1375 (2004).

S7. S. Clemett, C. Maechling, R. Zare, P. Swan, R. Walker, Science 262, 721 (1993).

S8. S. J. Clemett, R. N. Zare, in Proceedings of the IAU Symposium 178: Molecules in Astrophysics: Probes & Processes, E. F. Van Dishoeck, Ed. (Kluwer, Dordrecht, 1997), pp. 305-320.

S9. S. Clemett et al., Origins of Life and Evolution of the Biosphere 28, 425 (1998).

S10. D. P. Glavin et al., Meteoritics Planetary Science 41, 889 (2006).

S11. J. Kirz et al., Review of Scientific Instruments 63, 557 (1992).

S12. A. L. D. Kilcoyne et al., J. Synchrotron Radiation 10, 125 (2003)

S13. M. Lerotic et al., Journal of Electron Spectroscopy and Related Phenomena 144-147C, 1137 (2005).

S14. S. A. Sandford, R. M. Walker, R. M., Astrophys. J. 291, 838 (1985).

S15. L. J. Allamandola, S. A. Sandford, B. Wopenka, Science 237, 56 (1987).

S16. G. J. Flynn, L. P. Keller, M. Feser, S. Wirick, C. Jacobsen, Geochim. Cosmochim. Acta. 67, 4791 (2003).

S17. G. Matrajt et al., Astron. & Astroph. 433, 979 (2005).

S18. A. Rotundi et al., Workshop on Dust in Planetary Systems, in press.

S19. G. W. Cooper M. H. Thiemens, T. Jackson, S. Chang, Science 277, 1072 (1997).

S20. T. Stephan, Planet. Space Sci. 49, 859 (2001).

S21. K. D. McKeegan, R. M. Walker, E. Zinner, Geochimica et Cosmochimica Acta 49, 1971 (1985).

S22. P. Hoppe et al., Meteoritics Planetary Science 41, 197 (2006).

S23. M. Spencer, R. N. Zare, LPSC XXXVIII, 1432 (2006).

S24. M. J. Burchell, J. A. Creighton, A. T. Kearsley, Journal of Raman Spectroscopy 35, 249 (2004).

S25. J. Elsila, et al., Geochimica et Cosmochimica Acta 69(5), 1349 (2005).

S26. L. J. Kovalenko et al., Anal. Chem. 64, 682 (1992).

S27. J. H. Hahn, R. Zenobi, J. L. Bada, R. N. Zare, Science 239, 1523 (1988).

S28. R. Zenobi et al., Geochim. Cosmochim. Acta 56, 2899 (1992).

S29. D. S. McKay et al., Science 273, 924 (1996).

S30. S. Messenger et al., Astrophys. J. 502, 284 (1998).

S31. M. P. Bernstein et al., Science 283, 1135 (1999).

S32. T. Stephan, A. L. Butterworth, F. Hörz, C. J. Snead, A. J. Westphal, Meteoritics Planetary Science 41, 211 (2006).

S33. T. Stephan, E. K. Jessberger, C. H. Heis, D. Rost, Meteoritics Planetary Science 38, 109 (2003).

S34. J. Jacobsen, G. J. Flynn, S. Wirick, C. Zimba, Journal of Microscopy 197, 173 (2000).

S35. J. Stohr, NEXAFS Spectroscopy, (Springer Series in Surface Sciences, E. Gomer, Ed., New York, 1992).

S36. H. Busemann et al., Science 312, 727 (2006).

S37. M. E. Zolensky et al, this issue.

38. Acknowledgements –
The Organics PET is grateful for support and samples provided by the NASA Stardust Discovery Mission and the NASA Stardust Participating Scientist Program, and the wonderful support of the Stardust curatorial staff at Johnson Space Center, especially Keiko Nakamura-Messenger, Ron Bastien, Jack Warren, and Tom See.

Gas Chromatography/Mass Spectrometry work on the collected gas samples was done in the Toxicology Laboratory, Habitability and Environmental Factors Division, NASA-Johnson Space Center. The authors are particularly grateful for the efforts of M. Martin (Catholic University of America), V. de Vera (WYLE Laboratories), J. Boyd (WYLE Laboratories), T. Limero (WYLE Laboratories), and J. James (NASA-JSC).

Part of this work was performed under the auspices of the US Department of Energy by the Lawrence Livermore National Laboratory under Contract No. W-7405-ENG-48 and the Advanced Light Source, which is supported by the Director, Office of Science, Office of Basic Energy Sciences, Materials Sciences Division, of the U.S. Department of Energy under Contract No. DE-AC03-76F00098 at Lawrence Berkeley National Laboratory. We would like to thank Michael C. Martin and Z. Hao (LBNL) for their support at the beamline.

The Italian LANDS is grateful for support provided by the Università degli Studi di Napolit “Parthenope” and the Instituto Nazionale di Astrofisica.